High-Surface Step Density on Dendritic Pd Leads to Exceptional Catalytic Activity for Formic Acid Oxidation

S. Patra,[†] B. Viswanath,[‡] K. Barai,[§] N. Ravishankar,*[,‡] and N. Munichandraiah*[,†]

Department of Inorganic and Physical Chemistry, Materials Research Center, and Institute Nanoscience Initiative, Indian Institute of Science, Bangalore 560012, India

ABSTRACT Dendritic Pd with corrugated surfaces, obtained by a novel AC technique, exhibits an exceptionally high catalytic activity for the oxidation of formic acid because of the presence of a high density of surface steps. The formation of twinned dendrites leads to a predominance of exposed 111 facets with a high density of surface steps as evident from high resolution electron microscopy investigations. These surface sites provide active sites for the adsorption of the formic acid molecules, thereby enhancing the reaction rate. Control experiments by varying the time of deposition reveal the formation of partially grown dendrites at shorter times indicating that the dendrites were formed by growth rather than particle attachment. Our deposition method opens up interesting possibilities to produce anisotropic nanostructures with corrugated surfaces by exploiting the perturbations involved in the growth process.

KEYWORDS: step density • Pd dendrite • electrocatalytic activity • formic acid oxidation • AC technique • electrodeposition

Limited resources of Pt metal and issues with CO poisoning have prompted search for non-Pt fuel cell catalysts with high catalytic properties (1). In this context, Pd is a promising catalyst for direct formic acid fuel cell (DFAFC) because of its higher tolerance for CO poisoning than the Pt-based catalysts (2). Pd nanoparticles with different sizes and shapes have been investigated for their catalytic activity for a variety of reactions. The introduction of defect sites on surfaces is an interesting approach to enhance catalytic activity. The presence of surface defects such as steps/kinks are known to influence the kinetics of several reactions and provide active sites for adsorption and/or reaction (3). For instance, increasing step density on Pt nanoparticles enhanced specific activity up to 200% toward the electro-oxidation of CO and methanol (3a). Here we report a facile procedure for electrosynthesis of Pd dendritic nanostructures on carbon paper with a high density of surface steps by a novel ac method and demonstrate its high catalytic activity toward formic acid oxidation. The present electrochemical synthesis route, where an ac bias is applied over the dc potential of 0.1 V (see Materials and Methods), produces Pd nanostructures that exhibit an exceptionally high electrocatalytic activity for formic acid oxidation. The sinusoidal ac potential leads to an increase in defects, notably twins and surface steps that contribute to the high electrocatalytic activity. Twinning leads to the formation of predominantly {111} exposed facets with a high step density as illustrated in the schematic in Figure 1A. Electrodeposition of Pd using the ac technique results in the formation of branched dendrites on the carbon paper electrode. The uniform and dense coating of Pd nanostructures on the fibers of carbon paper is evident from the secondary electron SEM images B and C in Figure 1.

Detailed microstructural investigations using TEM (Figure 1D,E) clearly reveal the corrugated dendritic structure with the crystallographic analysis indicating that most of the dendrite branches grow along the ⟨110⟩ directions and that they consist of twins as illustrated in the schematic in Figure 1A (also, Figure 3D). This type of twinned growth has been observed in the case of Ag nanorods also and it has been proposed that breaking of symmetry leads to the formation of one-dimensional Ag nanostructure (4), which facilitates the formation of 111 facets as the bounding side facets in the nanostructure. The formation of a tapered structure in a dendrite implies that the 111 facet has a high surface step density to accommodate the change in diameter. The presence of nanoscale corrugations on the surface also translates to a high step density on the 111 facets as is evident from the high-resolution image in Figure 1E.

Powder XRD (Figure 2A) shows the dendrites correspond to FCC Pd (JCPDS file no.46−1043) with the peaks at $2\theta =$ 40.1, 46.7, 68.1, and 82.2° corresponding to the (111), (200), (220), and (222) planes of Pd, respectively. The peaks observed at $2\theta = 42.7$, 54.6, 77.5 and 86.8° are attributed to carbon. X-ray photoelectron spectrum (Figure 2B) corresponding to Pd (3d) indicates the presence of Pd in two different oxidation states (0 and +2) with the predominance of the metallic state. The presence of oxide is probably due to the surface oxidation of Pd dendrites as it was prepared under ambient conditions (see methods and materials in Experimental Section). From the thermogravimetric analysis

* Corresponding author. E-mail: muni@ipc.iisc.ernet.in (N.M.); nravi@mrc.iisc.ernet.in (N.R.).
Received for review July 25, 2010 and accepted October 21, 2010
[†] Department of Inorganic and Physical Chemistry, Indian Institute of Science.
[‡] Materials Research Center, Indian Institute of Science.
[§] Institute Nanoscience Initiative, Indian Institute of Science.
DOI: 10.1021/am100647u

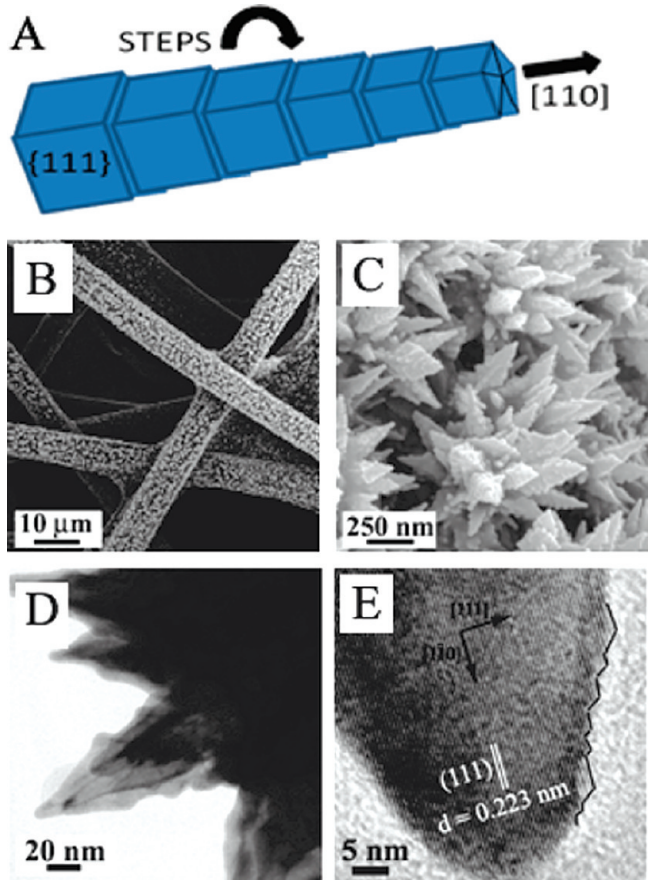

FIGURE 1. (A) Schematic illustration of the twinned dendritic structures formed by electrodeposition. The dendrites are bound by 111 facets with a high density of surface steps. (B) Low-magnification SEM image showing uniform coverage on carbon fibers. (C) Higher-magnification SEM image showing the dendritic nature of the Pd deposit. (D, E) TEM images showing corrugated surface structure with high step density on the surface.

(Figure 2C), the loading of Pd was estimated based on the complete decomposition of carbon paper into CO_2 at 866 °C. From the TGA curve, the amount of PdO residue was estimated to be 1% by weight, indicating that the loading of Pd was less than 1%.

A series of images illustrating the evolution of the Pd dendrites as a function of time is presented in Figure 3. It is seen that the growth of the dendrite starts from nearly equiaxed nanoparticles that branch out forming dendrites. The formation of dendritic structures by instabilities at the growth front has been studied in great detail (5) in the context of solidification. We believe that the instabilities in this case are induced by the sinusoidal potential applied during deposition as such structures are not seen in the case of DC deposition under similar conditions. The early stage particles are twinned and thus the dendrites inherit the twins from these particles during their growth as seen in the high resolution image (Figure 3D).

The electrocatalytic activity of the Pd dendrites was investigated for the electro-oxidation of formic acid as a model system. Figure 4A shows cyclic voltammogram of Pd/C electrode in 0.5 M HCOOH in 0.1 M H_2SO_4 at a sweep rate of 10 mV s^{-1}. Cyclic voltammogram of the electrode in the supporting electrolyte (without HCOOH) is also presented for comparison. The shape of the voltammogram of the dendritic Pd/C is as expected for Pd with the existence of one forward oxidation peak (P_a) at −0.03 V and two backward oxidation peaks (P_{b1}) at −0.1 and P_{b2} at 0.42 V, respectively (6). The peak P_a corresponds to the direct oxidation of formic acid leading to the formation of CO_2 as the end product (7). The peaks P_{b1} and P_{b2} are due to the oxidation of formic acid on the free active surface sites after reduction of PdO (6). Similarly, formic acid oxidation on single crystalline Pd (111) also showed two backward peaks (6a). The anodic and cathodic peaks in the range of 0.4 to 0.8 V are present in both the cyclic voltammograms in Figure 4a and arise due to the oxidation of Pd to PdO_2 and reduction of PdO_2 to Pd (8).

A comparative study of chemically prepared nanoporous Pd electrode (The SEM image of nanoporous Pd is given in the Supporting Information (Figure SI1)) and electrochemically prepared dendritic Pd/C electrode by cyclic voltammetry (Figure 5) reveals that the oxidation of formic acid on dendritic Pd/C electrode takes place at a potential considerably lower (∼165 mV) than that on the nanoporous Pd/C electrode and other similar nanostructures (9). The activity of commercial Pd/C catalyst was reportedly retarded by the formation of Pd oxide layer and peak potential for oxidation was 0.7 V (10). Wang et al. also reported a peak potential of 0.18 V vs SCE for the oxidation of formic acid on commercial Pd (Pd BASF) catalyst (8). The quantitative comparison of peak current is difficult because of different loading levels of catalyst. We propose that the dendritic Pd/C electrode is catalytically more favorable for electro-oxidation of formic acid primarily due to the presence of surface steps and twinning that leads to exposed {111} facets. At steps, atoms have lower co-ordination and are generally more reactive than atoms on a flat surface (11). The peak (P_{a2}) (Figure 5A, curve (ii)) due to oxidation of CO_{ad} is not observed in case of dendritic Pd which suggests that no fouling species formed on the surface (12). This is probably due to the presence of kink sites at the steps that not only increase the total reaction rate of formic acid electro-oxidation but also enhance the selectivity toward direct pathway in sulfuric acid as given by $HCOOH_{ad} \rightarrow CO_2 + 2H^+ + 2e^-$ (13). It is seen in voltammogram (Figure 5A, curve (i)) that the current peaks are narrow centered at about 0.0 V while sweeping both forward and backward directions. Ratio of area under forward oxidation peak (A_a) and backward oxidation peak (at higher potential) (A_b) indicates the activity of the electrode at lower potential. An A_a/A_b ratio of 3.6 was calculated for dendritic Pd as compared to 1.5 for nanoporous Pd electrode indicating a higher activity of the dendritic Pd at a lower potential.

For formic acid oxidation, the transient mass specific current density of dendritic Pd/C electrode at 0.4 V (to ensure full oxidation) is enhanced 4-fold as compared to the specific current density for oxidation on nonporous Pd/C (Figure 4B). The transient shows the stability of Pd catalyst over a period of 20 000 s. The SEM image of dendritic Pd/C taken after the chronoamperometry experiment does not show any sign

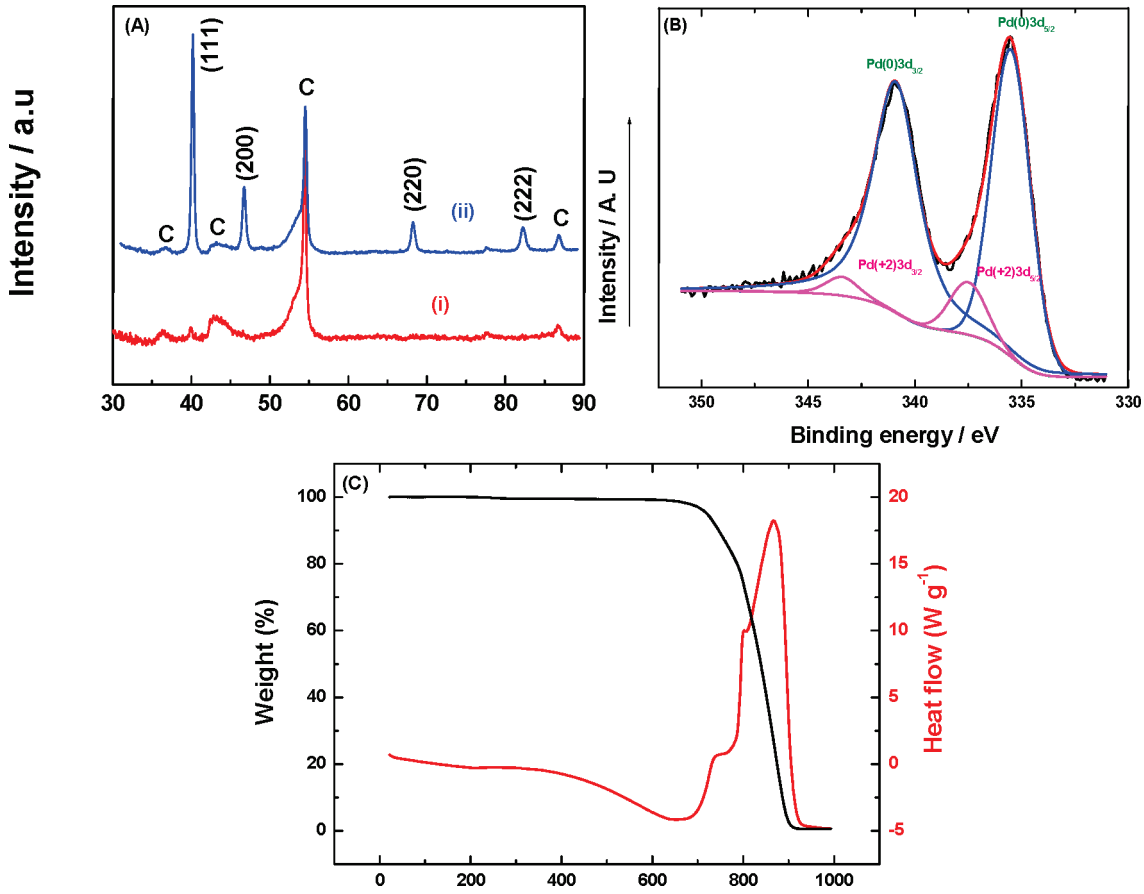

FIGURE 2. (A) X-ray diffraction pattern of (i) C and (ii) dendritic Pd/C; (B) X-ray photoelectron spectroscopy (XPS) of dendritic Pd/C indicating the presence of small amount of +2 oxidation state of Pd, and (C) TGA-DTA data of dendritic Pd/C electrode.

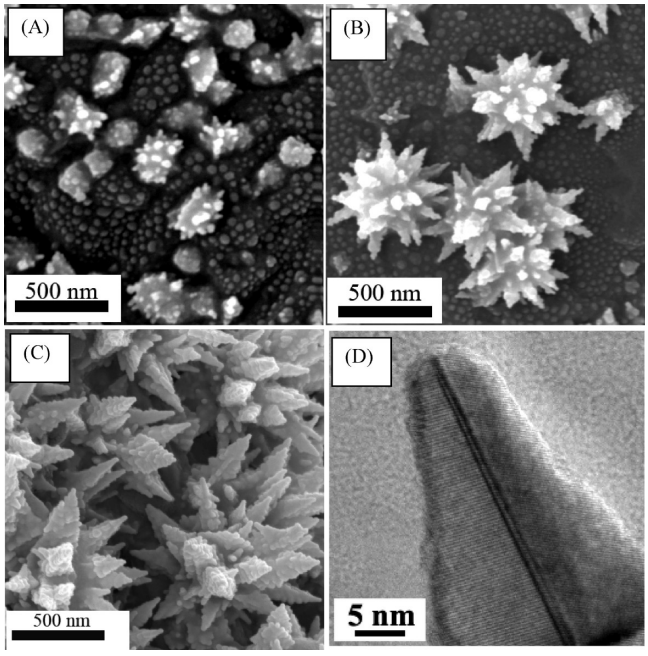

FIGURE 3. Secondary electron SEM images of dendrites Pd at the initial stages of growth for (A) 1, (B) 3, and (C) 5 min of deposition time, keeping concentrations of $PdCl_2$, temperature (22 °C), dc potential (0.1 V), and AC bias (50 mV) constant. (D) High-resolution TEM image of the Pd branch showing the presence of twin boundary parallel to the growth direction.

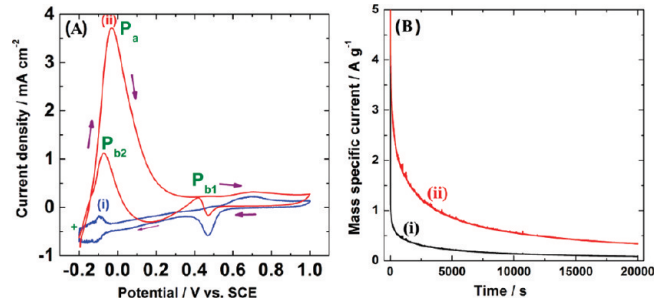

FIGURE 4. (A) Representative cyclic votammograms of dendritic Pd/C electrode at a sweep rate of 10 mV s^{-1} in (i) 0.1 M H_2SO_4 (without HCOOH) and (ii) in 0.5 M HCOOH and 0.1 M H_2SO_4; and (B) Chronoamperometry of (i) nanoporous Pd/C and (ii) dendritic Pd/C electrode in 0.5 M HCOOH and 0.1 M H_2SO_4 at 0.4 V.

of degradation of morphology. Concentration dependent linear sweep voltammetry of dendritic Pd/C is presented in Figure 5B which confirms that the peak P_a at −0.03 V is indeed due to the oxidation of formic acid. The cyclic voltammogram of dendritic Pd in 3 M HCOOH is given in the Supporting Information (Figure SI2) illustrates the potential application of the catalyst in formic acid fuel cells.

In summary, we have synthesized branched dendritic Pd with corrugated surfaces showing high catalytic activity toward formic acid oxidation reaction. We believe that the high electrocatalytic behavior of dendritic Pd is due to the corrugated surface nature of the Pd branches that possess a high step density that provides active sites for the adsorption of the formic acid, thereby enhancing the reaction rate. The ac deposition method for controlling surface structure to

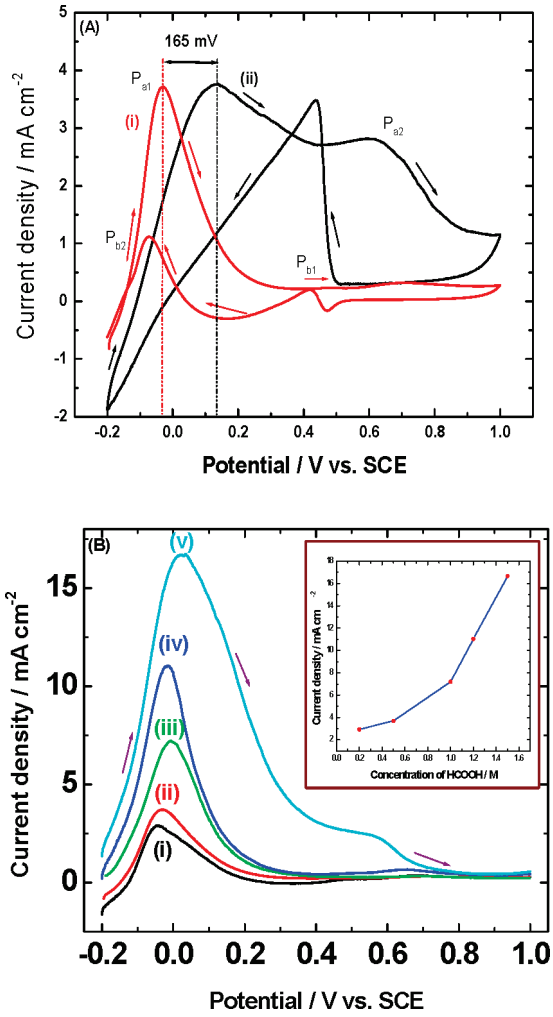

FIGURE 5. (A) Comparative cyclic voltammogram at a sweep rate of 10 mV s^{-1} of (i) dendritic Pd/C and (ii) nanoporous Pd/C electrode in 0.5 M HCOOH and 0.1 M H_2SO_4 shows the electrocatalytic behavior of dendritic Pd over nanoporous Pd for formic acid oxidation keeping their oxidation current constant. (B) Linear sweep voltammograms of dendritic Pd/C electrode at a sweep rate of 10 mV s^{-1} in 0.1 M H_2SO_4 with (i) 0.2, (ii) 0.5, (iii) 1, (iv) 1.2, and (v) 1.5 M of HCOOH demonstrate the increase in concentration of formic acid, the oxidation current increases which implies the peak at −0.03 V is due to oxidation of formic acid. The current density versus concentration of formic acid is shown in the inset of B.

enhance catalytic activity opens up interesting possibilities to produce anisotropic nanostructures for catalysis and other related applications.

EXPERIMENTAL SECTION

Materials and Methods. $PdCl_2$ was purchased from Aldrich. $NaBH_4$ and NaCl were purchased from Merck. A Toray carbon paper foil (thickness: 0.2 mm) was used as the substrate for electrodepositon of Pd. All solutions were prepared in doubly distilled water. A foil of 0.7 cm in width and 3.0 cm in length was sectioned out of a carbon paper, 1.4 cm^2 area at one of the ends was exposed to the electrolyte and the rest of its length was used to take electrical contact through a Cu wire. The unexposed area was masked with a PTFE tape to ensure that the electrolyte contacts only the required area. A glass cell of about 50 mL capacity with suitable ground-glass joints to introduce a working electrode (carbon paper electrode as mentioned above), Pt foil auxiliary electrodes, and a saturated calomel reference electrode (SCE) was used for electrochemical deposition and characterization studies. All potential values are reported against SCE. For electrochemical deposition of dendritic Pd on a carbon paper electrode, a solution of 0.01 M $PdCl_2$ and 0.01 M NaCl in 0.1 M H_2SO_4 was used as electrolyte. Pd dendrites on carbon paper were electrodeposited by an AC impedance technique where an ac voltage of 50 mV (frequency range was from 10 mHz to 100 kHz) was applied with a dc voltage of 0.1 V vs SCE. For chemical synthesis of nanoporous Pd, a solution of 0.01 M $PdCl_2$ and 0.01 M NaCl was added drop by drop to a stirring solution of $NaBH_4$. The resulting solid of Pd metal was collected by filtering and dried in the oven of 50 °C during an overnight. Nanoporous Pd was mixed with nafion and isopropyl alcohol to make slurry. The slurry was coated on a Toray carbon paper. The electrodes were dried and then weighed.

Characterization. AC deposition of Pd as well as cyclic voltammetry experiments were carried out using an EG&G PARC potentiostat/galvanostat model Versastat or a Solartron electrochemical interface model SI 1287. Microstructural investigations were carried out using field-emission gun scanning electron microscope (Sirion) and transmission electron microscope (TEM, TECNAI T20). X-ray diffraction (XRD) patterns were recorded using Philips diffractometer model X'PERT PRO using CuK_α ($\lambda = 1.5418$ Å) as the source. XPS studies were recorded using SPECS photoelectron spectrometer with Mg as the source and data were analyzed by Casa XPS software. While samples consisting of carbon paper coated electrodes were used for XRD, SEM and XPS investigations, electrodes were sonicated in acetone to disperse the coated materials and then drop-cast onto carbon coated Cu grids for TEM analysis. The TGA experiment was carried out in oxygen atmosphere under the flow rate of 100 mL/min and heating rate of 10 °C/min from room temperature to 1000 °C. All experiments were conducted in an air-conditioned room at 22 ± 1 °C.

Supporting Information Available: Additional figures (PDF). This material is available free of charge via the Internet at http://pubs.acs.org.

REFERENCES AND NOTES

(1) Wang, B. *J. Power Sources* **2005**, *152*, 1–5.
(2) Larsen, R.; Ha, S.; Zakzeski, J.; Masel, R. I. *J. Power Sources* **2005**, *144*, 28–34.
(3) (a) Lee, S. W.; Chen, S.; Sheng, W.; Yabuuchi, N.; Kim, Yong-T.; Mitani, T.; Vescovo, E.; Shao-Horn, Y. *J. Am. Chem. Soc.* **2009**, *131*, 15669–15677. (b) Somorjai, G. A.; Blakely, D. W. *Nature* **1975**, *258*, 580. (c) Banholzer, W. F.; Masel, R. I. *J. Catal.* **1984**, *85*, 127. (d) Housmans, T. H. M.; Koper, M. T. M. *J. Phys. Chem. B* **2003**, *107*, 8557–8567. (e) Lebedeva, N. P.; Koper, T. M.; Feliu, J. M.; Van Santen, R. A. *J. Phys. Chem. B* **2002**, *106*, 12938–12947.
(4) (a) Chen, H.; Gao, Y.; Zhang, H.; Liu, L.; Yu, H.; Tian, H.; Xie, S.; Li, J. *J. Phys. Chem. B* **2004**, *108*, 12038. (b) Lofton, C.; Sigmund, W. *Adv. Funct. Mater.* **2005**, *15*, 1197. (c) Halder, A.; Kundu, P.; Viswanath, B.; Ravishankar, N. *J. Mater. Chem.* **2010**, *20*, 4763–4772.
(5) Mullins, W. W.; Sekerka, R. F. *J. Appl. Phys.* **1963**, *34*, 323–329.

(6) (a) Baldeuf, M.; Kolb, D. M. *J. Phys. Chem.* **1996**, *100*, 11375–11381. (b) Meng, H.; Sun, S.; Masse, J.-P.; Dodelet, J.-P. *Chem. Mater.* **2008**, *20*, 6998–7002.
(7) Liu, Z.; Zhang, X. *Electrochem. Commun.* **2009**, *11*, 1667–1670.
(8) Wang, J.-Y.; Kang, Y.-Y.; Yang, H.; Cai, W.-B. *J. Phys. Chem. C* **2009**, *113*, 8366–8372.
(9) (a) Lee, H.; Habas, S. E.; Somorjai, G. A.; Yang, P. *J. Am. Chem. Soc.* **2008**, *130*, 5406–5407. (b) Liu, Z.; Hong, L.; Tham, M. P.; Lim, T. H.; Jiang, H. *J. Power Sources* **2006**, *161*, 831–835. (c) Wang, R.; Liao, S.; Ji, S. *J. Power Sources* **2008**, *180*, 205–208.
(10) Mazumder, V.; Sun, S. *J. Am. Chem. Soc.* **2009**, *131*, 4588–4589.
(11) (a) Boudart, M. *Adv. Catal.* **1969**, *20*, 153. (b) Hammer, B.; Norskov, J. K. *Adv. Catal.* **2000**, *45*, 71. (c) Lebedeva, N. P.; Koper, M. T.; Herrero, E.; Feliu, J. M.; Van Santen, R. A. *J. Electroanal. Chem.* **2000**, *487*, 37. (d) Hoshi, N.; Kida, K.; Nakamura, M.; Nakada, M.; Osada, K. *J. Phys. Chem. B* **2006**, *110*, 12480–12482. (e) Kasatki, I.; Kurr, P.; Kniep, B.; Trunschke, A.; Schlogl, R. *Angew. Chem., Int. Ed.* **2007**, *46*, 7324–7327.
(12) Li., H.; Sun, G.; Jiang, Q.; Zhu, M.; Sun, S.; Xin, Q. *Electrochem. Commun.* **2007**, *9*, 1410–1415.
(13) Lai, S. C. S.; Lebedeva, N. P.; Honsmans, T. H. M.; Koper, M. T. M. *Top. Catal.* **2007**, *46*, 320–333.

AM100647U